

Capillary fluctuations and energy dynamics for flow in porous media

James E. McClure

Virginia Polytechnic Institute & State University, Blacksburg

Steffen Berg

Shell Global Solutions International B.V. Grasweg 31, 1031HW Amsterdam, The Netherlands

Ryan T. Armstrong

University of New South Wales, Sydney

(Dated: July 7, 2022)

Capillary energy barriers have important consequences for immiscible fluid flow in porous media. We derive time-and-space averaging theory to account non-equilibrium behavior and understand the role of athermal capillary fluctuations and their relationship to phenomenological equations for multiphase flow. The formulation resolves several key challenges associated with two-fluid flow in porous media: (1) geometric and thermodynamic quantities are constructed as smooth functions of time based on time-and space averages; (2) averaged thermodynamics are developed for films; (3) multi-scale fluctuation terms are identified, which account for transient behaviours of interfaces and films that occur due to pore-scale events; (4) a criterion for representative elementary volume (REV) is established based on capillary fluctuations; (5) geometric constraints are derived and imposed on the averaged thermodynamics; and (6) a new constitutive model is proposed for capillary pressure dynamics that includes contributions from fluctuations. Based on the derived definitions, capillary fluctuations are assessed quantitatively based on pore-scale simulations and experimental core-flooding data.

PACS numbers: 05.70.Ln, 05.40.-a, 05.70.Np, 68.03.Cd, 47.56.+r

The non-equilibrium response to fluid flow through porous materials is inextricably linked to the length and time scales for processes that occur within the solid micro-structure [1–3]. It is well known that fluid pressures fluctuate during immiscible displacement as a consequence of pore-scale events [4–6]. The associated fluctuations are athermal and cooperative in nature based on the fact that they arise due to the influence of capillary forces during fluid displacement [7]. Theoretical treatment of these fluctuations is of central importance to modeling due to the fact that athermal fluctuations may not obey detailed balance [8]. Since the reversibility of molecular interactions is central to the development of Onsager’s non-equilibrium theory, the validity of phenomenological equations depends on the the properties of fluctuations within the system [9, 10]. The validity of near-equilibrium approximations and Onsager’s theory has been an important assumption in many theoretical developments for two-fluid flow in porous media [11–15].

When multiple length scales are present within a system, accompanying timescales will arise when considering the system dynamics. The linkage between temporal, spatial and energy scales is summarized in Fig. 1. Since information cannot propagate instantaneously, processes that occur over small length scales will tend to be more rapid compared to those that occur over larger length scales. Given a particular length scale, the energy scale relates to the work needed to move matter and energy the requisite distance. The rate that information propagates in the system is intrinsically linked to the phenomenolog-

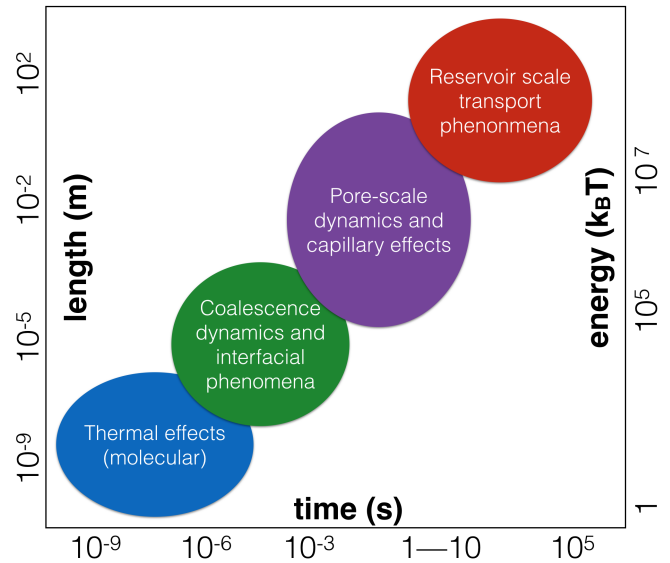


FIG. 1. Length and time scales for operative processes for multiphase flows in porous media. Geometric effects directly link smaller-scale phenomena with larger scale phenomena.

ical coefficients associated with particular physical processes. With respect to the validity of linear response theory, Onsager’s theory holds remarkably well in small systems, implying that local near-equilibrium approximations are usually reasonable [16]. At small length scales, near-equilibrium approximations are expected to fail only in extreme cases, such as in the immediate vicin-

ity of shock waves [17]. However, as the length scale associated with a process increases, so too does the required timescale to reach equilibrium. For immiscible fluids in a geological setting, the timescale required for diffusive processes to reach equilibrium is remarkably slow, with the timescale being measured in years for Ostwald ripening in CO₂-brine systems [18]. Within this context, slow physics represent a critical consideration when applying near-equilibrium assumptions at macroscopic length scales. The slow relaxation of diffusive systems explains the near-ubiquitous failure of Fick’s law in porous media [19–22]. While the timescale associated with capillary fluctuations is measured in seconds, the timescale to reach equilibrium can be hours to days in experimental systems [23]. It is therefore of great interest to develop non-equilibrium theory that does not rely on macroscopic near-equilibrium assumptions. In this paper we develop such a theory.

For multiphase flows in porous media, we identify three length scales of primary interest: (1) the interfacial length scale associated with the width of the interface (10-50nm); (2) the pore length scale associated with the representative length scale for the solid microstructure (nm-mm); and (3) the Darcy length scale associated with macroscopic flow processes through porous media (cm - km). For each length scale, particular processes of interest can be identified. At the interface length scale, film swelling effects can occur due to flow; coalescence events occur based on the merging of two fluid regions, which form loops or otherwise alter the topology of the fluid [24]. Fluid singularities result from the associated disruption to the interface mean curvature [25–38]. Snap-off events are also common in typical flow processes [39]. At the pore length scale, Haines jumps occur when fluid spontaneously fills regions of the the pore structure as fluids migrate between capillary energy barriers [40]. These microscopic events are a primary source of non-equilibrium behavior, and are therefore a focus area when considering the physical meaning of near equilibrium approximations. The length scale of interest for flow processes is the Darcy scale, typically orders of magnitude larger than that of the pore scale.

In the following sections we provide a conceptual overview of the basic physical considerations needed to model immiscible displacement in porous media. Formal theoretical development proceeds in six steps: (1) definition of the thermodynamic system; (2) averaging in time-and-space; (3) rate of external work in Darcy-scale systems; (4) derivation of geometric constraints; (5) multi-scale analysis for capillary fluctuations; and (6) formulation of flux-force entropy and derivation of phenomenological equations for two-phase flow. The derivation leads to explicit criteria for the validity of phenomenological equations based on the structure of capillary fluctuations in the system. Using results from simulation and experimental data, we directly evaluate the derived capillary

fluctuation terms and consider the consequences for REV definition and the development of averaged descriptions for two-fluid flow in porous media.

BACKGROUND

At the pore scale capillary forces are dominant and determine how fluids are distributed within the solid microstructure. Capillary pressure accounts for the contribution of surface forces that arise due to the meniscus curvature and surface energy [41]. The Young-Laplace equation relates the pressure difference between the adjoining fluids and the capillary pressure given by the product of the interfacial tension γ and mean curvature:

$$p_n - p_w = \gamma_{wn} \left(\frac{1}{R_1} + \frac{1}{R_2} \right). \quad (1)$$

where R_1 and R_2 are the principal curvature radii at points on the fluid meniscus. The Laplace equation holds only at mechanical equilibrium, and does not account for dynamic processes that involve moving interfaces. This necessarily includes any process where the fluid volumes change, since these changes can only occur based on movement of the interface. Situations arise where interface movement occurs at constant volume, such as capillary waves. To describe these cases it is necessary to understand the non-equilibrium response of the fluid pressures based on the capillary dynamics within the system.

As fluids squeeze through the microstructure of complex materials while influenced by capillary forces, rapid changes to the fluid configuration occur as the system jumps between metastable states. The displacement can be sub-divided into a sequence of *isons* and *rheons* [4, 5]. The associated events are depicted in Fig. 2. Isons correspond to reversible displacement events where the fluid meniscus invades a pore throat under quasi-static conditions, i.e. the fluid pressure difference is balanced by the capillary forces in the throat. The fluid pressure difference increases proportionate to the meniscus curvature as the interface is pushed into increasingly narrow parts of the pore throat. When the meniscus moves through the narrowest part of the pore neck, pore-filling occurs spontaneously based on an event often known as a Haines jump [40]. As the meniscus curvature decreases, the fluid pressure difference significantly exceeds the capillary pressure and fluid rapidly fills the pore. This irreversible event is known as a *rheon*. Pore-filling events that transpire as Haines jumps can dissipate a significant amount of energy [1, 2]. Furthermore, they occur very quickly (milliseconds to seconds) compared to typical laboratory- and reservoir-scale process (hours to weeks). Considering large systems, processes of interest involve very large numbers of such events. Understanding their overall effect is of central importance to under-

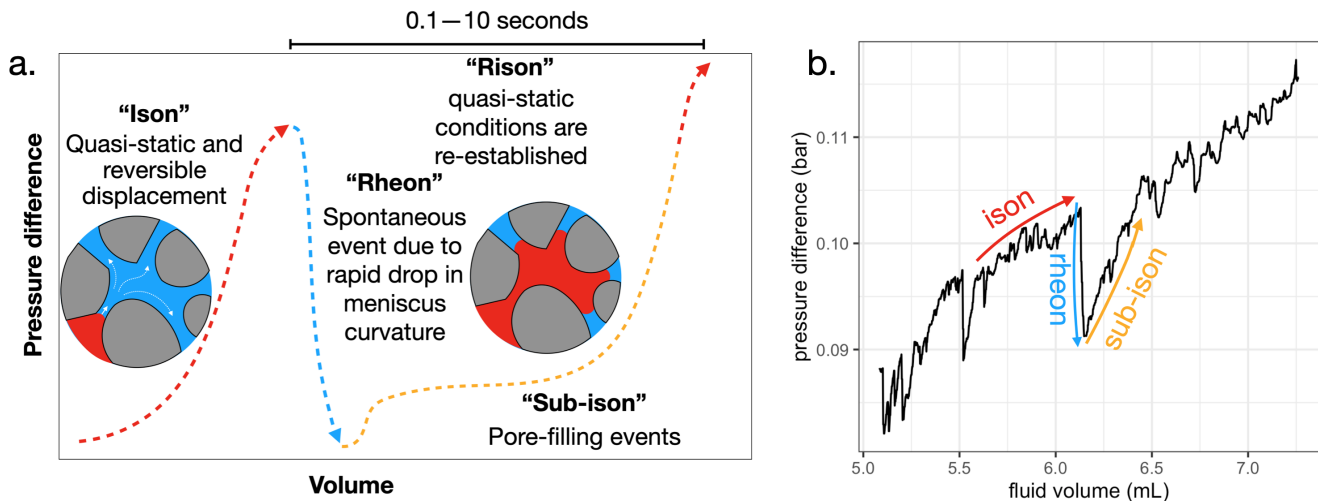


FIG. 2. Pore-scale displacement events can be separated into reversible events called *isons* and irreversible *rheons* (a) Isons correspond to reversible displacement as the capillary pressure increases, forcing the fluid meniscus into narrower pore throats. When the meniscus passes through the narrowest part of the pore-throat, energy is released during the ensuing pore-filling event. A rapid drop in capillary pressure occurs as the meniscus curvature decreases, which corresponds to a rheon. Fluid then spontaneously fills the pore until the local capillary pressure is again balanced by the fluid pressure difference; (b) identification of ison, rheon and sub-ison events from experimental data.

standing transient effects for multiphase flows in porous media.

The dissipation from pore-scale events can be estimated from basic concepts of work and energy. A typical experiment can be treated as a system where external work is performed in two primary ways. First is the work associated with fluid flow. The volumetric flow rate is \mathbf{Q}_i for each fluid $i \in \{w, n\}$ results due to external work performed on the system by some external potential gradient $\nabla\Phi_i$, e.g. due to an external pressure gradient or body force. Since work is defined as the applied force multiplied by the distance, the total rate of work is

$$\frac{dW_{darcy}}{dt} = \nabla\Phi_i \cdot \mathbf{Q}_i. \quad (2)$$

Conceptually, the work due to Darcy flow occurs in a steady-state system, meaning that there are no net changes to the internal energy, with each fluid forming static connected pathways through the sample that allow flow to occur. The conventional relative permeability relationship predicts the flux per area as

$$\mathbf{q}_i = -\frac{k_{ri}}{\mu_i} \mathbf{K} \cdot \nabla\Phi_i, \quad (3)$$

where $\mathbf{q}_i = \mathbf{Q}_i/A$, k_{ri} is the relative permeability, μ_i is the dynamic viscosity and \mathbf{K} is the permeability tensor for the material. This can be combined with Eq. 2 to approximate the rate of work based on an applied external potential gradient.

Pressure-volume work occurs when one fluid displaces another. Considering a wetting and non-wetting fluid

with pressure p_w and p_n , this contribution to the external work is given by

$$\frac{\partial W_{ext}}{\partial t} = (p_w - p_n) \frac{\partial V_w}{\partial t}. \quad (4)$$

External work performed on the system is transferred to the internal energy of the system or dissipated as heat. Changes to the surface energy account for a significant part of the external pressure-volume work. If the solid material is water-wet, the change in surface energy is proportional to the change in surface area based on the interfacial tension γ_{wn} . Morrow therefore defined the displacement efficiency as the fraction of pressure-volume work that is converted to surface energy [5]

$$E_d = \frac{\gamma_{wn} \Delta A_{wn}}{\int (p_w - p_n) dV_w}, \quad (5)$$

where A_{wn} is the boundary surface for the non-wetting fluid. Seth and Morrow showed that the efficiency for a primary drainage varies from 10–95% depending on the material type [42]. The dissipated energy can also be estimated from the mechanistic picture illustrated in Fig. 2. The pressure-volume work associated with an initial *ison* can be considered to be reversible based on the fact that the displacement is quasi-static. Since a rheon is spontaneous, the work associated with the ensuing sub-ison accounts for the dissipated energy after any surface energy changes generated by the event has been subtracted.

Models for capillary pressure dynamics in porous media have been previously developed to account for the macroscopic behaviour during displacement. The first such models were developed using concepts of work and

energy [5]. Subsequent models incorporated concepts of non-equilibrium thermodynamics [11, 15] and kinematics [13, 43]. Previously developed models fail to deal with the challenges associated with the non-smooth response of the fluid pressure and interfacial curvature. This critical challenge is associated with changes to the fluid topology, which necessarily cause a discontinuity in the interfacial curvature [24, 30, 37]. The apparent geometric discontinuity links to questions about whether or not multi-fluid systems can be considered to be in a near-equilibrium state. Bear & Nitao argue that while relatively simple macroscopic thermodynamic equations of state must exist at equilibrium due to the Gibbs phase rule, these relations will break down under non-equilibrium conditions if the mean-square deviation is too large [14]. For systems with slow physics, near equilibrium conditions can break down as the length scale for the REV increases due to the larger timescale required for mixing to occur. In this work, we consider how multi-scale effects influence the transient capillary pressure behavior and consider consequences for the rate of energy dissipation. Multi-scale fluctuation terms are identified explicitly, which can be directly evaluated and compared to other energy dynamics within the system. Conditions derived based on these fluctuation terms clearly demonstrate when Onsager theory can be applied to derive phenomenological models such as the conventional relative permeability relationship. A new expression for the dynamic capillary pressure is also derived, which directly includes effects due to fluctuations. Capillary fluctuations are then directly evaluated based on pore-scale simulations and experimental data.

THEORETICAL APPROACH

In the following sections we present the theoretical approach used to derive constitutive models for immiscible fluid flow through porous media. Our approach relies on averaging in both time and space, which is distinct from previously developed models. Capillary fluctuation terms are included explicitly, and special treatment is needed to develop a flux-force entropy inequality that accounts for capillary fluctuations. The flux-force form of the entropy inequality can be exploited to derive standard expressions for relative permeability as well as a dynamic capillary pressure relationship that includes the effect of *rheons* and *isons* during unsteady displacement. The theoretical approach is organized into six steps:

1. **Thermodynamic description** – variables required to formulate a classical thermodynamic description of the pore-scale system, including effects due to fluid phases, interfaces and films;
2. **Thermodynamic averages in space and time** – averaging is applied to develop thermodynamic

forms that hold at larger length and time scales. Fluctuation terms arise as a consequence of averaging in both space and time.

3. **Rate of work and entropy inequality** – an entropy inequality is developed by defining the rate of external work associated with fluid flow;
4. **Geometric constraints** – a geometric constraint is needed to relate the time derivative for the interfacial area to the time derivative for the fluid volume fractional. A relationship between partial derivatives for geometric quantities is derived;
5. **Capillary fluctuations** – a multi-scale expansion is developed to associate fluctuation terms to steady-state or unsteady displacement, which is needed to derive a flux-force form for the entropy inequality;
6. **Flux-force form of entropy inequality** – all results are combined to form a flux-force form of the entropy inequality. A REV constraint is derived for the fluctuations. Provided the constraint is met, standard relative permeability relationships are obtained as well as a form to approximate the capillary pressure dynamics during unsteady displacement.

By explicitly considering the contribution from fluctuations in the flux-force of the entropy inequality, conditions for the validity of derived phenomenological equations can be developed explicitly. These conditions do not rely on the assumption of detailed balance. Instead they are requirements for how fluctuations must behave so that phenomenological equations can provide a valid representation for the entropy production in the system. Experimental data is then used to assess the role of capillary fluctuations in the context of the theory.

Thermodynamic Description

Thermodynamics provides a mechanism to link flow processes with conservation of energy. For non-equilibrium systems, this is accomplished by deriving an expression for the entropy production, which can then be exploited to derive phenomenological equations for particular processes [10]. At the practical level, thermodynamics is a multi-scale book-keeping system to keep track of how energy is distributed within a system. Entropy production occurs when energy is transferred from macroscopic energy modes (such as pressure-volume work) to thermal modes that are linked to the system entropy based on the molecular degrees of freedom. The thermodynamics of heterogeneous systems are typically treated by sub-dividing the system into sub-regions based

on the system composition [12, 44, 45]. In addition to the entropy S we consider the extensive variables to be

- V_i – fluid volume for $i \in \{w, n\}$
- A_n – surface area for fluid n
- A_s – surface area for the solid material
- h_s – film thickness along the solid material
- N_{ik} – number of molecules of type k within any region $i \in \{w, n, s\}$

Energy associated with the solid is omitted for simplicity, such as effects associated with deformation. The surface area bounding the wetting fluid A_w is omitted based on the fact that only two of $\{A_n, A_w, A_s\}$ are independent. The internal energy is given as a function of the independent extensive quantities

$$U = U(S, V_w, V_n, A_n, A_s, h_s, N_{ak}, N_{bk}, N_{sk}) . \quad (6)$$

The Euler equation for the internal energy of the system is then written as

$$U = TS - p_w V_w - p_n V_n + \gamma_{wn} A_n + \gamma_s A_s + \Pi_s h_s A_s + \mu_{ak} N_{ak} + \mu_{bk} N_{bk} + \mu_{sk} N_{sk} , \quad (7)$$

where the intensive measures are

- p_i – fluid pressure for $i \in \{w, n\}$
- γ_{wn} – surface energy for fluid-fluid interface
- γ_s – surface energy for the solid material
- Π_s – disjoining pressure along the solid material
- μ_{ik} – chemical potential for molecule k within any region $i \in \{w, n, s\}$

In a strongly wetted system, the solid surface is coated everywhere by a thin film of fluid w . This means that fluid n interacts with w everywhere along its boundary, described by the surface energy γ_{wn} . If the system is not strongly wetted by w , the formulation can still be used based on the fact that any excess energy due to interactions between the fluids and the solid will be accounted for by local variations in γ_s along the solid. The complexity of the fluid-solid interactions is therefore embedded within the associated energy terms. In our approach, we do not treat the solid as being in contact with a particular fluid. Instead we consider the situation where the associated interfacial energy γ_s and film thickness h_s can vary along the solid. The formulation presupposes that films coat the solid surface everywhere, with the understanding that if the film thickness $h_s = 0$ locally on portions of the solid surface, this will be equivalent to treating films

as covering only part of the solid surface. The disjoining pressure is therefore defined as

$$\Pi_s \equiv \frac{1}{A_s} \left(\frac{\partial U}{\partial h_s} \right)_{S, V_w, V_n, A_n, A_s, N_{ak}, N_{bk}, N_{sk}} \quad (8)$$

The energy due to fluid-solid interactions is therefore lumped into two terms, one associated with the interfacial energy and a second due to the disjoining pressure and film contributions. Variations in γ_s and h_s along the surface of the solid occur due to the interaction between the fluid and solid material, including the effects of roughness and chemical heterogeneity.

The terms that account for capillary fluctuations are neglected in conventional non-equilibrium thermodynamics; these appear only when time-averaged thermodynamics are introduced. From the physical perspective, time averaging is needed to account for the path of the system in its entirety. When considering flow processes that occur over long periods of time, it is easy to overlook fast dynamics. Haines jumps are one such category of event, with dynamics that typically occur over a duration of milliseconds to seconds [2, 46, 47]. Topological changes such as droplet coalescence also dissipate energy, occurring even more rapidly and contributing to pressure fluctuations. While both classes of event are common for flows in porous media, the associated energy dissipation has not been properly included in thermodynamic models. In the following sections, we demonstrate that pressure fluctuations represent an essential contribution to the energy dynamics for two-fluid flow in porous media.

Thermodynamic Averages in Space and Time

The use of time averaging to study non-equilibrium behavior for two-fluid flow in porous media was first treated by Aryana and Kavscek [48]. While these authors demonstrated that the conventional Buckley-Leverett model could be derived based on this approach (as well as extended models), aspects pertaining to the non-equilibrium thermodynamics were not considered. Here we develop this theory explicitly. Averages are constructed with the time-and-space averaging operator, defined as

$$\langle f \rangle \equiv \frac{1}{\lambda \mathcal{V}} \int_{\Lambda} \int_{\Omega} f dV dt , \quad (9)$$

where Λ is a region of time with duration λ and Ω is a spatial averaging region [49]. \mathcal{V} is the volume associated with thermodynamic measurements. For example, if the fluid pressure is measured with a transducer, \mathcal{V} represents the volume of fluid that can be considered as being in equilibrium with the measured value. The total volume of Ω is $V > \mathcal{V}$. In the context of ergodic theory, the averaging operator given by Eq. 9 explicitly

mixes information in space and time to generate averages. Non-ergodic effects can be accounted for in the averaged system provided that Λ and Ω are chosen appropriately. Averages of the extensive quantities are simple averages so that these quantities retain their basic meaning

$$\begin{aligned} \bar{S} &\equiv \langle S \rangle, & \bar{V}_i &\equiv \langle V_i \rangle, & \bar{N}_{ik} &\equiv \langle N_{ik} \rangle, \\ \bar{A}_i &\equiv \langle A_i \rangle, & \bar{h}_s &\equiv \langle h_s \rangle, \end{aligned} \quad (10)$$

The intensive measures are then defined to maintain scale-consistency with Eq. 7

$$\begin{aligned} \bar{T} &\equiv \frac{\langle TS \rangle}{\langle S \rangle}, & \bar{p}_i &\equiv \frac{\langle p_i V_i \rangle}{\langle V_i \rangle}, & \bar{\mu}_{ik} &\equiv \frac{\langle \mu_{ik} N_{ik} \rangle}{\langle N_{ik} \rangle}, \\ \bar{\gamma}_i &\equiv \frac{\langle \gamma_i A_i \rangle}{\langle A_i \rangle}, & \bar{\Pi}_s &\equiv \frac{\langle \Pi_s A_s h_s \rangle}{\langle A_s h_s \rangle}. \end{aligned} \quad (11)$$

The internal energy in the averaged thermodynamic model will then be given by

$$\begin{aligned} \bar{U} &= \bar{T}\bar{S} - \bar{p}_w \bar{V}_w - \bar{p}_n \bar{V}_n + \bar{\gamma}_{wn} \bar{A}_n + \bar{\gamma}_s \bar{A}_s + \bar{\Pi}_s \bar{A}_s \bar{h}_s \\ &\quad + \bar{\mu}_{ak} \bar{N}_{ak} + \bar{\mu}_{bk} \bar{N}_{bk} + \bar{\mu}_{sk} \bar{N}_{sk}. \end{aligned} \quad (12)$$

Statistical definitions for thermodynamic quantities rely on the ergodic hypothesis such that ensemble averages are the same as averages in space or time. The basis for this assumption is that the molecules are locally well-mixed, i.e. that the molecules in the system interact and exchange energy on a timescale that is sufficiently fast relative to the size of the system considered. Within this context Eq. 7 holds in the limit of infinite time and non-equilibrium expressions must be developed to study time-dependent processes. In a non-equilibrium system, deviations of the intensive quantities contribute to the energy dynamics [49]. The deviation terms are defined as the difference between the microscopic value and the averaged value

$$\begin{aligned} T' &\equiv T - \bar{T}, & p'_i &\equiv p_i - \bar{p}_i, & \mu'_{ik} &\equiv \mu_{ik} - \bar{\mu}_{ik}, \\ \gamma'_i &\equiv \gamma_i - \bar{\gamma}_i, & \Pi'_s &\equiv \Pi_s - \bar{\Pi}_s. \end{aligned} \quad (13)$$

The time derivative for the internal energy includes contributions from the time derivatives of the averages of the extensive measures as well as fluctuation terms that arise due to the microscopic deviations in the intensive quantities

$$\begin{aligned} \frac{\partial \bar{U}}{\partial t} &= \bar{T} \frac{\partial \bar{S}}{\partial t} - \bar{p}_w \frac{\partial \bar{V}_w}{\partial t} - \bar{p}_n \frac{\partial \bar{V}_n}{\partial t} + \bar{\mu}_{ik} \frac{\partial \bar{N}_{ik}}{\partial t} + \bar{\gamma}_{wn} \frac{\partial \bar{A}_n}{\partial t} \\ &\quad + (\bar{\gamma}_s + \bar{\Pi}_s \bar{h}_s) \frac{\partial \bar{A}_s}{\partial t} + \bar{\Pi}_s \bar{A}_s \frac{\partial \bar{h}_s}{\partial t} - \left\langle S \frac{\partial T'}{\partial t} \right\rangle \\ &\quad + \left\langle V_w \frac{\partial p'_w}{\partial t} \right\rangle + \left\langle V_n \frac{\partial p'_n}{\partial t} \right\rangle - \left\langle N_{ik} \frac{\partial \mu'_{ik}}{\partial t} \right\rangle, \\ &\quad - \left\langle A_n \frac{\partial \gamma'_{wn}}{\partial t} \right\rangle - \left\langle A_s \frac{\partial \gamma'_s}{\partial t} \right\rangle - \left\langle A_s h_s \frac{\partial \Pi'_s}{\partial t} \right\rangle, \end{aligned} \quad (14)$$

where a sum is implied for all chemical potential terms. The multi-scale fluctuation terms account for transient effects and heterogeneity associated with the thermodynamic behaviour:

- $\left\langle V_i \frac{\partial p'_i}{\partial t} \right\rangle$ – fluid pressure fluctuations, e.g. due to the transient effect of changing capillary forces on the fluid pressure during flow;
- $\left\langle A_n \frac{\partial \gamma'_{wn}}{\partial t} \right\rangle$ – fluctuations to the fluid-fluid interfacial tension, e.g. due to different surface tension along the fluid-fluid interface, which may arise if surfactants are present;
- $\left\langle A_s \frac{\partial \gamma'_s}{\partial t} \right\rangle$ – fluctuations to the fluid-solid surface energy, e.g. which occur due to movement of the contact line and complex fluid-solid interactions that occur due to surface heterogeneity;
- $\left\langle A_s h_s \frac{\partial \Pi'_s}{\partial t} \right\rangle$ – fluctuations to the disjoining pressure of films on the solid surface, e.g. which can occur due to localized film swelling;
- $\left\langle N_{ik} \frac{\partial \mu'_{ik}}{\partial t} \right\rangle$ – fluctuations to chemical potential, which can arise due to any diffusive process.

There is a direct link between the pressure fluctuation defined in Eq. 14, and associated rugged energy landscapes. The reversible work associated with an *ison* is captured based on the product of the fluid pressure difference and rate of volume change, as in standard non-equilibrium thermodynamics. During a strictly quasi-static displacement, the rate of change for the microscopic pressure p_i should closely correspond with the average fluid pressure \bar{p}_i . On the other hand, if we consider a *rheon* to be a rapid pressure change at constant volume, then p_i must deviate significantly from \bar{p}_i over the duration of the event. Therefore, if there are *rheons* occurring within Ω during the time interval Λ then the associated fluctuation terms are expected to have a significant effect. Pressure fluctuation terms contribute to the non-equilibrium description based on pore-scale events that transpire within the averaging window defined by Λ and Ω . This will be treated in more detail in sections to follow.

Rate of work and entropy inequality

The change to the internal energy of the system is determined based on the rate of work done on the system and the heat added

$$\frac{\partial \bar{U}}{\partial t} = \frac{\partial \bar{W}}{\partial t} + \frac{\partial \bar{Q}}{\partial t}. \quad (15)$$

The instantaneous rate of work is given by the sum of Eqs. 2 and 4, the latter being already built into the

thermodynamics. For the data considered in this work, which correspond to immiscible two-fluid flow in strongly water-wet systems, several assumptions can be made to simplify the form of Eq. 14:

1. the system temperature is uniform and no heat is added to the system

$$T = \bar{T} \rightarrow \left\langle S \frac{\partial T'}{\partial t} \right\rangle = 0, \quad \frac{\partial Q}{\partial t} = 0;$$

2. the fluid-fluid interfacial tension is constant everywhere:

$$\gamma_{wn} = \bar{\gamma}_{wn} \rightarrow \left\langle A_n \frac{\partial \gamma'_{wn}}{\partial t} \right\rangle = 0;$$

3. the solid does not change shape, meaning that

$$\frac{\partial \bar{A}_s}{\partial t} = 0, \quad \frac{\partial \bar{V}_w}{\partial t} = -\frac{\partial \bar{V}_n}{\partial t};$$

4. compositional effects can be ignored

$$\bar{\mu}_{ik} \frac{\partial \bar{N}_{ik}}{\partial t} = 0, \quad \left\langle N_{ik} \frac{\partial \mu'_{ik}}{\partial t} \right\rangle = 0.$$

Subject to these assumptions and using Eq. 15 to replace the change to the internal energy with the rate of external work done on the system, Eq. 14 can be simplified and rearranged to obtain an entropy inequality

$$\begin{aligned} \frac{\partial \bar{S}}{\partial t} = \frac{1}{\bar{T}} & \left\{ \underbrace{\nabla \bar{\Phi}_w \cdot \bar{\mathbf{Q}}_w + \nabla \bar{\Phi}_n \cdot \bar{\mathbf{Q}}_n}_{\text{work of fluid flow}} \right. \\ & + V \left[\underbrace{(\bar{p}_w - \bar{p}_n) \frac{\partial \bar{\phi}_w}{\partial t}}_{\text{ison}} - \underbrace{\left\langle \phi_w \frac{\partial p'_w}{\partial t} + \phi_n \frac{\partial p'_n}{\partial t} \right\rangle}_{\text{rheon}} \right] \\ & - \underbrace{\bar{\gamma}_{wn} \frac{\partial \bar{A}_n}{\partial t} + \left\langle A_s \frac{\partial \gamma'_s}{\partial t} \right\rangle}_{\text{change in surface energy}} \\ & \left. - \underbrace{\bar{A}_s \bar{\Pi}_s \frac{\partial \bar{h}_s}{\partial t} + \left\langle A_s h_s \frac{\partial \Pi'_s}{\partial t} \right\rangle}_{\text{film swelling}} \right\} \geq 0, \end{aligned} \quad (16)$$

where the fluid volume fraction and associated time-average are

$$\phi_i = \frac{V_i}{V}, \quad \bar{\phi}_i = \frac{\bar{V}_i}{V} \quad \text{for } i \in \{w, n\}. \quad (17)$$

In the context of Fig. 2, specific terms appear that correspond with the reversible pressure-volume work associated with an *ison* and the spontaneous *rheons*. Three fluctuation terms are retained, the first associated with capillary fluctuations in the fluid pressures. The second is due to wetting fluctuations that are attributed to the

movement of the contact line during fluid displacement, which appears due to the time derivative for the deviation of the solid interaction energy γ'_s . Intuitively, the fluid-solid interaction energy changes when the common line moves. Finally, the effects of film swelling contribute based on the fluctuation of the disjoining pressure, which will change based on changes to the film thickness. This contribution is important primarily when the wetting fluid is poorly connected, in which case films that coat the solid surface provide a primary flow pathway for that fluid. To obtain a more useful form of the entropy inequality, a flux-force form must be obtained [9]. In the following sections we demonstrate how this can be accomplished for systems where the fluctuation terms play a significant role.

Geometric constraints

As fluid is injected into a porous material, the configuration of fluids within the microstructure changes, with interfaces rearrangement occurring alongside displacement. Changes to the fluid volume fraction will typically also lead to changes in interfacial area. However, since interfacial area can change without any change to the volume fraction, the chain rule cannot be applied to simplify Eq. 16,

$$\frac{\partial \bar{A}_n}{\partial t} \neq \frac{\partial \bar{A}_n}{\partial \bar{\phi}_w} \frac{\partial \bar{\phi}_w}{\partial t}.$$

The rate of change in surface area is neither independent from the rate of change in the volume fraction, nor entirely dependent on it. To obtain a flux-force form of the entropy inequality, the dependent component must be distinguished from the independent component. It has been previously showed that a global geometric relationship can be constructed based on a non-dimensional relationship developed based on invariant measures of integral geometry [24]. Here we apply this relationship to the time-and-space averaged geometric measures

$$f(\bar{\phi}_n, \bar{W}_n, \bar{X}_n) = 0. \quad (18)$$

The non-dimensional measures are defined as

$$\bar{W}_n = \frac{\bar{A}_n^2}{H_n V}, \quad X_n = \frac{\bar{\chi}_n \bar{A}_n}{H_n^2}. \quad (19)$$

where \bar{A}_n is the time average for the surface area of the non-wetting fluid boundary, \bar{H}_n is the time average of integral mean curvature, and $\bar{\chi}_n$ is the time average for the Euler characteristic. Even though the instantaneously measured χ_n is a discontinuous function of time, $\bar{\chi}_n$ will be continuous due to its construction as a time average. While the Gibbs dividing surface can be considered as

introducing non-smooth aspects into the system description based on the discrete representation of fluid regions according to set theory, the time-and-space average removes any non-smooth behaviors by incorporating the past and future state of the system within the instantaneous representation. To link the time derivatives for the surface area and volume fraction, we note that a differential form is implied by Eq. 18

$$\frac{\partial \phi_n}{\partial t} = \frac{\partial \phi_n}{\partial \bar{W}_n} \frac{\partial \bar{W}_n}{\partial t} + \frac{\partial \phi_n}{\partial \bar{X}_n} \frac{\partial \bar{X}_n}{\partial t}. \quad (20)$$

Since \bar{W}_n and \bar{X}_n include \bar{A}_n , this can be arranged to remove the rate of change in surface area from Eq. 16. The link between thermodynamics and the geometric evolution can be understood by expanding the derivatives using the definitions in Eq. 19

$$\begin{aligned} \frac{\partial \bar{W}_n}{\partial t} &= \frac{\partial \bar{W}_n}{\partial \bar{A}_n} \frac{\partial \bar{A}_n}{\partial t} + \frac{\partial \bar{W}_n}{\partial \bar{H}_n} \frac{\partial \bar{H}_n}{\partial t} \\ &= \frac{2\bar{A}_n}{\bar{H}_n V} \frac{\partial \bar{A}_n}{\partial t} - \frac{\bar{A}_n^2}{\bar{H}_n^2 V} \frac{\partial \bar{H}_n}{\partial t}. \end{aligned} \quad (21)$$

Topological contributions arise based on the time derivative of \bar{X}_n

$$\begin{aligned} \frac{\partial \bar{X}_n}{\partial t} &= \frac{\partial \bar{X}_n}{\partial \bar{A}_n} \frac{\partial \bar{A}_n}{\partial t} + \frac{\partial \bar{X}_n}{\partial \bar{H}_n} \frac{\partial \bar{H}_n}{\partial t} + \frac{\partial \bar{X}_n}{\partial \bar{\chi}_n} \frac{\partial \bar{\chi}_n}{\partial t} \\ &= \frac{\bar{\chi}_n}{\bar{H}_n^2} \frac{\partial \bar{A}_n}{\partial t} - 2 \frac{\bar{\chi}_n \bar{A}_n}{\bar{H}_n^3} \frac{\partial \bar{H}_n}{\partial t} + \frac{\bar{A}_n}{\bar{H}_n^2} \frac{\partial \bar{\chi}_n}{\partial t}. \end{aligned} \quad (22)$$

Inserting the previous two expressions into Eq. 20 and rearranging terms leads to an expression that links the time derivatives

$$\frac{\partial \phi_n}{\partial t} = +g_1 \frac{\partial \bar{A}_n}{\partial t} - g_2 \frac{\partial \bar{H}_n}{\partial t} + g_3 \frac{\partial \bar{\chi}_n}{\partial t}, \quad (23)$$

where three geometric functions have been defined as follows, each of which are determined based on the geometric state of the system

$$g_1 = \frac{2\bar{A}_n}{\bar{H}_n V} \frac{\partial \phi_n}{\partial \bar{W}_n} + \frac{\bar{\chi}_n}{\bar{H}_n^2} \frac{\partial \phi_n}{\partial \bar{X}_n}, \quad (24)$$

$$g_2 = \frac{\bar{A}_n^2}{\bar{H}_n^2 V} \frac{\partial \phi_n}{\partial \bar{W}_n} + 2 \frac{\bar{\chi}_n \bar{A}_n}{\bar{H}_n^3} \frac{\partial \phi_n}{\partial \bar{X}_n}, \quad (25)$$

$$g_3 = \frac{\bar{A}_n}{\bar{H}_n^2} \frac{\partial \phi_n}{\partial \bar{X}_n}. \quad (26)$$

The average curvatures for the surface can be obtained by dividing the integral mean curvature and Euler characteristic by the total surface area,

$$\bar{J}_n \equiv \frac{\bar{H}_n}{\bar{A}_n}, \quad \bar{K}_n \equiv \frac{\bar{\chi}_n}{\bar{A}_n}. \quad (27)$$

This means that

$$\frac{\partial \bar{H}_n}{\partial t} = \bar{J}_n \frac{\partial \bar{A}_n}{\partial t} + \bar{A}_n \frac{\partial \bar{J}_n}{\partial t}, \quad (28)$$

$$\frac{\partial \bar{\chi}_n}{\partial t} = \bar{K}_n \frac{\partial \bar{A}_n}{\partial t} + \bar{A}_n \frac{\partial \bar{K}_n}{\partial t}, \quad (29)$$

where the average mean curvature \bar{J}_n and average Gaussian curvature \bar{K}_n are now cast as intensive properties of the surface. Inserting into Eq. 23 and rearranging terms leads to

$$\begin{aligned} \frac{\partial \phi_n}{\partial t} &= \frac{\partial \bar{A}_n}{\partial t} (g_1 - g_2 \bar{J}_n + g_3 \bar{K}_n) \\ &\quad + \bar{A}_n \left(g_3 \frac{\partial \bar{K}_n}{\partial t} - g_2 \frac{\partial \bar{J}_n}{\partial t} \right), \end{aligned} \quad (30)$$

expanding terms we find that

$$g_2 \bar{J}_n = \frac{1}{\bar{J}_n V} \frac{\partial \phi_n}{\partial \bar{W}_n} + 2 \frac{\bar{\chi}_n}{\bar{H}_n^2} \frac{\partial \phi_n}{\partial \bar{X}_n} \quad (31)$$

and

$$g_3 \bar{K}_n = \frac{\bar{\chi}_n}{\bar{H}_n^2} \frac{\partial \phi_n}{\partial \bar{X}_n}, \quad (32)$$

which means that

$$g_1 - g_2 \bar{J}_n + g_3 \bar{K}_n = \frac{1}{\bar{J}_n V} \frac{\partial \phi_n}{\partial \bar{W}_n}. \quad (33)$$

Solving to eliminate the time derivative for the surface area as it appears in the thermodynamic expressions,

$$\begin{aligned} \frac{\partial \bar{A}_n}{\partial t} &= V \bar{J}_n \frac{\partial \bar{W}_n}{\partial \phi_n} \frac{\partial \phi_n}{\partial t} + \frac{\bar{A}_n}{\bar{J}_n} \frac{\partial \bar{J}_n}{\partial t} \\ &\quad - \frac{V}{\bar{J}_n} \frac{\partial \bar{W}_n}{\partial \bar{X}_n} \left(2 \frac{\bar{K}_n}{\bar{J}_n} \frac{\partial \bar{J}_n}{\partial t} - \frac{\partial \bar{K}_n}{\partial t} \right). \end{aligned} \quad (34)$$

Capillary Fluctuations

The multi-scale fluctuation terms that appear in Eq. 16 account for excess energy dissipation that is due to fast dynamics. In this section, we consider the role of capillary fluctuations in more detail, focusing on their contribution during unsteady displacement. Capillary fluctuations occur due to the geometric evolution of the fluids. As interfaces squeeze through the pore-space, exchanges between the pressure-volume energy and surface energy occur frequently. Of particular interest to our work are the fluctuation terms associated with the fluid pressures. The fluctuations in the fluid pressure are caused directly by changes to the interface shape due to the capillary forces, e.g. during Haines jumps and other fast dynamics. Critically, fluctuations in capillary pressure are very fast relative to the timescale for Darcy-scale phenomena, but also very slow compared to thermal fluctuations. When measured from the molecular length scale thermal effects

give rise to pressure fluctuations. These molecular effects relate to entropic degrees of freedom and the associated contribution to the internal energy is explicitly accounted for in Eq. 7. For the time-averaged non-equilibrium expressions, fluctuations in the pressure can occur due to capillary forces that are not linked with the thermal degrees of freedom in the system, and the associated energetic contributions must be retained to properly describe energy dynamics within the system.

We consider a multi-scale expansion to deal with the fundamental challenge associated with the fast timescale for pore-scale events and put Eq. 16 into a flux-force form. To construct the expansion, we identify a fast timescale that is associated with pore-level events and a slow timescale that is associated with macroscopic changes. It is generally accepted that pore-level events such as Haines jumps are responsible for the fluctuating pressures as depicted in Fig. 2. Mohanty et al. derive the timescale for the jump time as [46]

$$t_p = \sqrt{\frac{\rho D_p^3}{\gamma_{wn}}} . \quad (35)$$

A relevant macroscopic timescale is inversely proportional to the rate of change in fluid volume fraction. Since the rate of change for the fluid volume fraction is comparatively slow, we define the small parameter

$$\varepsilon_i = \frac{\partial \bar{\phi}_i}{\partial t} \sqrt{\frac{\rho D_p^3}{\gamma_{wn}}} . \quad (36)$$

Proceeding based on the method of multiple scales, we define the macroscopic timescale as

$$t_i^* = \varepsilon_i t . \quad (37)$$

The pressure deviation can now be expressed based the multi-scale expansion

$$p'_i(t) = p_i'^{(0)}(t, t_i^*) + \varepsilon_i p_i'^{(1)}(t, t_i^*) + \mathcal{O}(\varepsilon_i^2) , \quad (38)$$

Using Eqs. 36 and 37, the time derivative can now be written as

$$\frac{\partial p'_i}{\partial t} = \frac{\partial p_i'^{(0)}}{\partial t} + \sqrt{\frac{\rho D_p^3}{\gamma_{wn}}} \frac{\partial \bar{\phi}_i}{\partial t} \left(\frac{\partial p_i'^{(0)}}{\partial t_i^*} + \frac{\partial p_i'^{(*)}}{\partial t} \right) . \quad (39)$$

where the fast fluctuation is defined such that all terms that multiply ε_i are included,

$$\frac{\partial p_i'^{(*)}}{\partial t} = \frac{1}{\varepsilon_i} \left(\frac{\partial p'_i}{\partial t} - \frac{\partial p_i'^{(0)}}{\partial t} \right) . \quad (40)$$

The leading term is associated with the steady effect, i.e. due to rearrangements of the fluids that are due to the macroscopic flow regime. The second term accounts for

unsteady effects that are due to the change in saturation, which drives pore-scale events that occur at a fast timescale. For convenience the average fluctuation can be defined formally,

$$\bar{p}_i'^{(0)} \equiv \frac{1}{\bar{\phi}_i} \left\langle \phi_i \frac{\partial p_i'^{(0)}}{\partial t} \right\rangle , \quad (41)$$

$$\bar{p}_i'^{(*)} \equiv \frac{1}{\bar{\phi}_i} \left\langle \phi_i \left(\frac{\partial p_i'^{(0)}}{\partial t_i^*} + \frac{\partial p_i'^{(*)}}{\partial t} \right) \right\rangle , \quad (42)$$

which means that

$$\left\langle \phi_i \frac{\partial p'_i}{\partial t} \right\rangle = \bar{\phi}_i \left(\bar{p}_i'^{(0)} + \bar{p}_i'^{(*)} \sqrt{\frac{\rho D_p^3}{\gamma_{wn}}} \frac{\partial \bar{\phi}_i}{\partial t} \right) . \quad (43)$$

As above, the first term corresponds to pressure fluctuations that are inherently due to the flow regime, whereas the second term corresponds to faster timescale fluctuations due to pore-scale events. Note since ε_i includes the rate of change in volume fraction, the first term is the only term in the expansion that is not multiplied by $\partial \bar{\phi}_i / \partial t$. The effect is to determine which part of the pressure fluctuation should be affiliated with the steady-state relative permeability terms, and which should be attributed with unsteady effects.

The same multi-scale expansion approach can be applied to obtain an analogous form for the other fluctuation terms. In general, movement of the common line will alter the average fluid-solid surface energy $\bar{\gamma}_s$. These changes will also be associated with contributions from the associated fluctuation terms. However, in a strongly wetted system where the solid surface is coated everywhere by a thin fluid film, we can assume that the fluctuation term is not important because fluid-solid interaction energy is entirely due to the interaction of the water films and solid, i.e.

$$\frac{\partial \bar{\gamma}_s}{\partial t} = 0 . \quad (44)$$

However, in this situation swelling of the water films can alter the internal energy, and must therefore be accounted for in the thermodynamic description. Analogous to Eqs. 41 and 42, the film fluctuations are defined as

$$\bar{\Pi}_s'^{(0)} \equiv \frac{1}{\bar{A}_s \bar{h}_s} \left\langle A_s h_s \frac{\partial \Pi_s'^{(0)}}{\partial t} \right\rangle , \quad (45)$$

$$\bar{\Pi}_s'^{(*)} \equiv \frac{1}{\bar{A}_s \bar{h}_s} \left\langle A_s h_s \left(\frac{\partial \Pi_s'^{(0)}}{\partial t_i^*} + \frac{\partial \Pi_s'^{(*)}}{\partial t} \right) \right\rangle . \quad (46)$$

so that

$$\left\langle A_s h_s \frac{\partial \Pi'_s}{\partial t} \right\rangle = \bar{A}_s \bar{h}_s \left(\bar{\Pi}_s'^{(0)} + \bar{\Pi}_s'^{(*)} \sqrt{\frac{\rho D_p^3}{\gamma_{wn}}} \frac{\partial \bar{\phi}_i}{\partial t} \right) . \quad (47)$$

With scale separation now defined for the fluctuation terms, we can return to the entropy inequality to consider further developments.

Flux-force form of entropy inequality

Classical non-equilibrium theory relies on a flux-force form of the entropy inequality to derive phenomenological equations [10]. Using the fact that the molecular system is time-reversible, detailed balance is assumed in deriving linear phenomenological equations [9]. However, in systems with cooperative effects, such as interfacial rearrangements, detailed balance will not hold within sub-regions of the system occupied by individual fluids. The fluctuation terms are of central importance to this effect, since they capture the net contribution due to cooperative effects over Λ and Ω . As long as the fluctuations can be properly accounted for in the flux-force entropy inequality, phenomenological equations may be derived. Using the results of the previous sections, we now obtain such a result. We consider situations where changes to the film thickness are caused by changes to the fluid volume fraction,

$$\frac{\partial \bar{h}_s}{\partial t} = \frac{\partial \bar{h}_s}{\partial \phi_w} \frac{\partial \phi_w}{\partial t}. \quad (48)$$

Making use of Eqs. 43, 44, 47, 34 and 48 the entropy inequality in Eq. 16 can be put into a flux-force form

$$\begin{aligned} \frac{\partial \bar{S}}{\partial t} = \frac{V}{T} & \left\{ \frac{1}{V} \left(\underbrace{\nabla \bar{\Phi}_w \cdot \bar{\mathbf{Q}}_w + \nabla \bar{\Phi}_n \cdot \bar{\mathbf{Q}}_n}_{\text{Work of Darcy flow}} \right) \right. \\ & + \frac{\partial \phi_w}{\partial t} \left[\underbrace{\bar{p}_w - \bar{p}_n + \bar{\gamma}_{wn} \bar{J}_n \frac{\partial \bar{W}_n}{\partial \phi_w} + \frac{\bar{A}_s \bar{\Pi}_s}{V} \frac{\partial \bar{h}_s}{\partial \phi_w}}_{\text{pressure-volume work}} \right. \\ & \left. \left. - \sqrt{\frac{\rho D_p^3}{\gamma_{wn}}} \left(\underbrace{\bar{\phi}_w \bar{p}'_w^{(*)} - \bar{\phi}_n \bar{p}'_n^{(*)} - \frac{\bar{A}_s \bar{h}_s}{V} \bar{\Pi}'_s^{(*)}}_{\text{fast fluctuations}} \right) \right] \right. \\ & \left. - \underbrace{\bar{\phi}_w \bar{p}'_w^{(0)} - \bar{\phi}_n \bar{p}'_n^{(0)} + \frac{\bar{A}_s \bar{h}_s}{V} \bar{\Pi}'_s^{(0)} - \frac{\bar{\gamma}_{wn} \bar{A}_n}{\bar{J}_n V} \frac{\partial \bar{J}_n}{\partial t}}_{\text{slow fluctuations and surface energy}} \right. \\ & \left. + \underbrace{\frac{\bar{\gamma}_{wn}}{\bar{J}_n} \frac{\partial \bar{W}_n}{\partial \bar{X}_n} \left(2 \frac{\bar{K}_n}{\bar{J}_n} \frac{\partial \bar{J}_n}{\partial t} - \frac{\partial \bar{K}_n}{\partial t} \right)}_{\text{curvature evolution constraint}} \right\} \geq 0. \quad (49) \end{aligned}$$

Provided that Ω and Λ are sufficiently large, $\bar{\phi}_i$, \bar{a}_{wn} and \bar{J}_n will change slowly with time, which is due to the fact that they are time averages. The fast dynamics are entirely embedded within the associated fluctuation terms. Eq. 49 is not yet in a flux-force form due to the contribution from the slow fluctuations and the geometric evolution. For slow fluctuations, there may be reversible energy transfer from the pressure fluctuation terms to the

surface energy. This is expressed based on the constraint,

$$\begin{aligned} \bar{\phi}_w \bar{p}'_w^{(0)} + \bar{\phi}_n \bar{p}'_n^{(0)} - \frac{\bar{A}_s \bar{h}_s}{V} \bar{\Pi}'_s^{(0)} + \frac{\bar{\gamma}_{wn} \bar{A}_n}{\bar{J}_n V} \frac{\partial \bar{J}_n}{\partial t} \\ + \frac{\bar{\gamma}_{wn}}{\bar{J}_n} \frac{\partial \bar{W}_n}{\partial \bar{X}_n} \left(2 \frac{\bar{K}_n}{\bar{J}_n} \frac{\partial \bar{J}_n}{\partial t} - \frac{\partial \bar{K}_n}{\partial t} \right) = 0 \end{aligned} \quad (50)$$

This form should be considered from two perspectives: (1) steady-state flow at constant fluid volume fraction; and (2) unsteady flow where the the fluid volume fraction is changing. In a steady-state flow, the curvature must be independent of time, since any net change to the geometric configuration of fluids is inconsistent with the system being at steady-state. Therefore, the associated conditions are

$$\frac{\partial \bar{K}_n}{\partial t} = 0, \quad \frac{\partial \bar{J}_n}{\partial t} = 0, \quad (51)$$

$$\bar{\phi}_w \bar{p}'_w^{(0)} + \bar{\phi}_n \bar{p}'_n^{(0)} - \frac{\bar{A}_s \bar{h}_s}{V} \bar{\Pi}'_s^{(0)} = 0, \quad (52)$$

and there must be no net rate of energy change from fluctuations at steady-state, since otherwise the symmetry required for Onsager reciprocal theory will be violated. By construction the slow fluctuations correspond to those fluctuations that occur at constant volume fraction. For unsteady displacement, capillary fluctuations may be balanced by changes to the average curvature invariants, \bar{J}_n and \bar{K}_n . This reflects the fact that the fluid configuration can change at constant fluid volume fraction based on changes to the boundary curvature. Since the boundary curvature can evolve independently from the volume, a separate term must appear in the entropy inequality to account for these effects.

Since the terms in Eq. 50 do not multiply the change in fluid volume fraction in Eq. 49, it is essential that their average value be zero. Otherwise, the flux-force form of the entropy inequality cannot be exploited to derive phenomenological equations. Any net contribution from the fluctuation terms during steady-state fractional flow invalidates any corresponding measurement of the the relative permeability. On the other hand, if Eq. 50 is satisfied then the effective permeability coefficients can be considered to account for the dissipation that occurs during steady-state flow, including contributions from pore-scale events on the basis that the average rate of events does not change with time based on the averaging domain, Λ and Ω . Results obtained using pore-network models for steady-state fractional flow suggest that the associated fluctuations will be symmetric [7]. In this case a flux-force form is possible for Eq. 49, with the thermodynamic forces identified as

$$\nabla \bar{\Phi}_w, \quad \nabla \bar{\Phi}_n, \quad \frac{\partial \bar{\phi}_w}{\partial t}. \quad (53)$$

The resulting flux-force form of the entropy inequality can naturally be applied to derive the standard constitutive relationship for relative permeability, given in Eq.

3. This conventional relationship assumes that the relationship between the flow rate \bar{q}_i and the applied forces $\nabla\bar{\Phi}_i$ is linear, which is known to break down as the capillary number increases. This result is also based on the assumption that the forces and fluxes are independent, which has been called into question based on the results of homogenization theory [13, 50]. Previous efforts to derive Eq. 3 from first principles have generally concluded that the flow rates \bar{q}_w and \bar{q}_n are not independent due to momentum exchanges between the two fluids. For example, if an external potential gradient is applied only to one fluid, it will pull some amount of the other fluid along with it, which is not accounted for based on Eq. 3. Cross-coupling forms have been proposed to account for this effect [50, 67]. However, since cross-coupling forms introduce additional phenomenological parameters, it is considerably more complicated to measure experimentally and therefore difficult to apply in real systems. From the more practical standpoint, one can consider the k_{ri} as being a proxy for the dissipation rate; since the entropy is a scalar, we can always embed this rate within a scalar parameter. This conceptual picture is more consistent with how relative permeability is used in practice, since k_{ri} is usually considered to be a non-linear function of the capillary number, viscosity ratio and the pore-scale distribution of fluids [53]. More recent efforts align with this conceptual picture, and can be considered as characterizing the non-linear dependence of the dissipation rate on the applied forces [51].

The rate of change for the fluid volume fraction has been previously used to derive expressions for capillary pressure dynamics [11]. We obtain an alternate form that includes the effect of both films and capillary fluctuations

$$\frac{\partial\bar{\phi}_w}{\partial t} = \frac{1}{\tau_w} \left(\bar{p}_w - \bar{p}_n + \bar{\gamma}_{wn} \bar{J}_n \frac{\partial\bar{W}_n}{\partial\phi_w} + \frac{\bar{\Pi}_s \bar{A}_s}{V} \frac{\partial\bar{h}_s}{\partial\phi_w} - F_c^* \right), \quad (54)$$

where τ_w is a phenomenological parameter and F_c^* accounts for the energy contribution that is due to capillary fluctuations

$$F_c^* \equiv \sqrt{\frac{\rho D_p^3}{\gamma_{wn}}} \left(\phi_w \bar{p}'_w^{(*)} - \phi_n \bar{p}'_n^{(*)} - \frac{\bar{A}_s \bar{h}_s}{V} \bar{\Pi}'_s^{(*)} \right). \quad (55)$$

Eq. 54 is an expression for the capillary pressure dynamics, which differs from previous forms in several important ways. First, the effect of film swelling is included, which is important for the snap-off mechanism. The capillary term includes the contribution over the entire fluid boundary, including the part of the boundary where the shape is strongly influenced by the local solid microstructure. Due to the effect of films, the force-balance in these regions differs from the meniscus. In the averaged form, the equilibrium requirement is that all force contributions must cancel, including the effect of the fluid pressures, meniscus curvature, and film contributions. Second, the capillary fluctuation terms defined by Eq. 55

are accounted for explicitly. Averaging in both time and space ensures smoothness of the pressure signal with respect to time provided that the system size and time interval for averaging are sufficiently large. It is possible that average contribution due to capillary fluctuations will vanish in REV-scale systems. For this to happen the positive and negative contributions must cancel. From the perspective of pore-scale events, Ω and Λ must be large enough to capture the distribution of events within a particular material. This will depend on both the material and the flow rate. However, the fluctuation term is not guaranteed to vanish because the capillary pressure signal is non-stationary. If the distribution of fast fluctuations is not symmetric about zero, then there will be a net energy contribution to capillary pressure dynamics that is due to capillary fluctuations. It is therefore important to treat the fluctuation terms cautiously. In the following sections, we consider several practical examples to illustrate the behaviour for capillary fluctuations and their contribution to the energy dynamics in multiphase systems.

RESULTS

Flow through porous media

The flow of immiscible fluids in porous media are strongly influenced by geometric and topological effects [55–63]. Capillary forces typically dominate such flows, and these forces are directly impacted by changes to fluid connectivity. We consider fluid displacement within a porous medium as a means to explore how geometric changes influence physical behavior. A periodic sphere packing was used as the flow domain. Using a collective rearrangement algorithm, eight equally-sized spheres with diameter $D = 0.52$ mm were packed into a fully-periodic domain $1 \times 1 \times 1$ mm in size. The system was discretized to obtain a regular lattice with 256^3 voxels. Simulations of fluid displacement were performed by injecting fluid into the system so that the effect of topological changes could be considered in detail. Initially the system was saturated with water, and fluid displacement was then simulated based on a multi-relaxation time (MRT) implementation of the color lattice Boltzmann model [65].

To simulate primary drainage, non-wetting fluid was injected into the system at a rate of $Q = 50$ voxels per timestep, corresponding to a capillary number of 4.7×10^{-4} . A total of 500,000 timesteps were performed to allow fluid to invade the pores within the system, forming the sequence of structures shown in Fig. 3 a–c. The first pores are invaded at $t = 0.19$ seconds, which is just after the system overcomes the entry pressure. The fluid does not yet form any loops, since a pore must be invaded from two different directions before a loop will be

created. Haines jumps and loop creation can be considered as distinct pore-scale events that may coincide in certain situations. At time $t = 0.34$ seconds the first loop is formed. As primary drainage progresses additional loops form such that the total curvature tends to decrease as non-wetting fluid is injected.

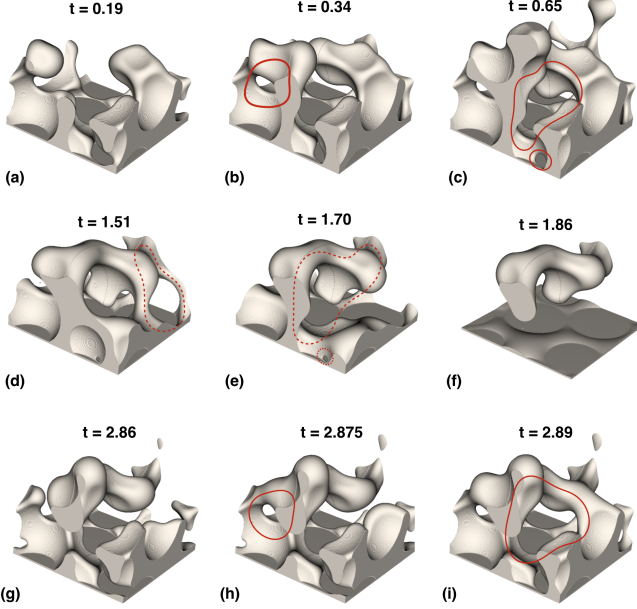


FIG. 3. Coalescence and snap-off events alter the topology of fluids within porous media: (a)-(c) pore-scale events such as Haines jumps lead to the formation of non-wetting fluid loops that are associated with coalescence events that occur during pore-filling; (d)-(f) imbibition destroys fluid loops due to snap-off, eventually trapping non-wetting fluid within the porespace; (h)-(i) trapped fluids reconnect during secondary drainage.

At the end of primary drainage the flow direction was reversed to induce imbibition, with water injected at a rate of $Q = 20$ voxels per timestep. Sequences from the displacement are shown in Fig. 3 d-f. As water imbibe into the smaller pores in the system, there is a well-known tendency to snap off non-wetting fluid between connections to larger adjacent pores where imbibition has not yet occurred. This is known as the Roof snap-off mechanism [39]. Snap-off breaks loops within the system, causing the Euler characteristic to increase. The order that loops snap off during imbibition is not the reverse of the order that the loops form during drainage. This is because the drainage process is dominated by the size of the throats whereas imbibition is governed by the size of the pores. Eventually, the sequence of snap-off events can cause non-wetting fluid to become disconnected from the main region, leading to trapping as seen at time $t = 1.86$ seconds.

The presence of trapped fluid distinguishes secondary drainage from primary drainage. The sequence of fluid configurations shown in Fig. 3 depicts the sequence of

coalescence events that reconnect trapped fluid. Due to the presence of trapped fluid, the order that loops are formed within the porespace does not match the order observed during primary drainage.

Primary and secondary drainage each show a rapid spike in the pressure difference due to the entry pressure. The entry sequence along primary drainage is labeled as A-C and matches the configurations from Fig. 4a. The high pore entry pressure is consistent with expected behavior that the largest energy barriers in the capillary dominated system are due to pore entry [2]. The pore entry sequence along secondary drainage is labeled H-J. On secondary drainage, the entry pressure is slightly reduced due to the presence of trapped fluid. This shows that the first coalescence event depicted in Fig. 3a-c corresponds exactly to the maximum fluid pressure difference observed during pore entry. This is distinct from the initial pore entry observed during primary drainage, because it is the fluid coalescence event that cause the fluid pressures to fluctuate.

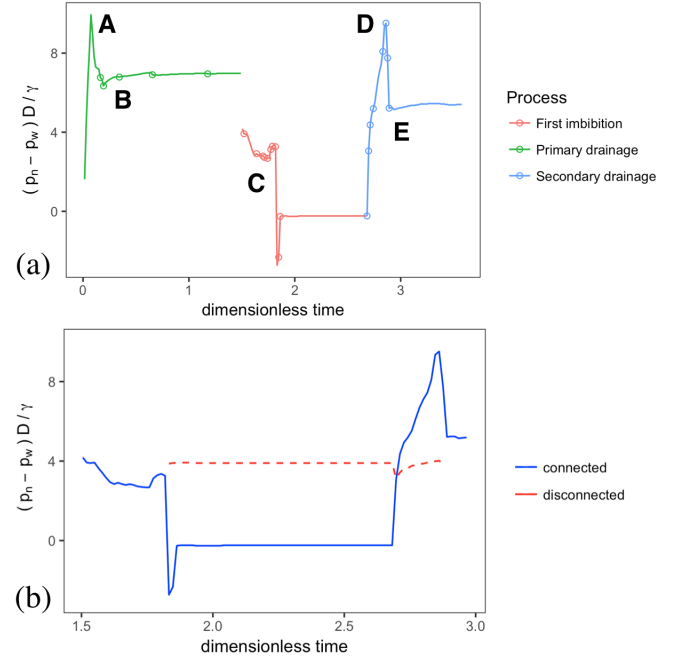


FIG. 4. Response of the capillary pressure to connectivity events: (a) the difference between the pressure of the connected water and non-wetting fluid show that non-smooth disruptions to the capillary pressure landscape align with connectivity events identified by changes in Euler characteristic (circles); (b) snap-off causes large disruptions in capillary pressure, with non-wetting fluid trapped at higher capillary pressure than the bulk fluid.

Like coalescence, snap-off events are associated with clear fluctuations in the bulk fluid pressures. The snap-off sequence shown in Fig. 3 is labeled as D-F in Fig. 4. As loops of fluid are destroyed, corresponding fluctuations in the fluid pressure difference are observed.

The largest disruption is associated with the snap-off event. The capillary pressure for the connected and disconnected regions of non-wetting fluid is shown in Fig. 4b. Consistent with the observation of other authors, fluid is trapped at a higher capillary pressure than what is measured in the connected fluid phases at the instant of snap-off [39]. As soon as snap-off occurs, the time derivative of the pressure difference between the two connected fluid phases immediately jumps from strongly negative to strongly positive. This occurs as each fluid region relaxes toward its preferred equilibrium state, which is possible because the two fluid regions are no longer mixing after the snap-off event. The final pressure for the trapped region is determined based on geometry, with the fluid assuming a minimum energy configuration within the pores where it is trapped.

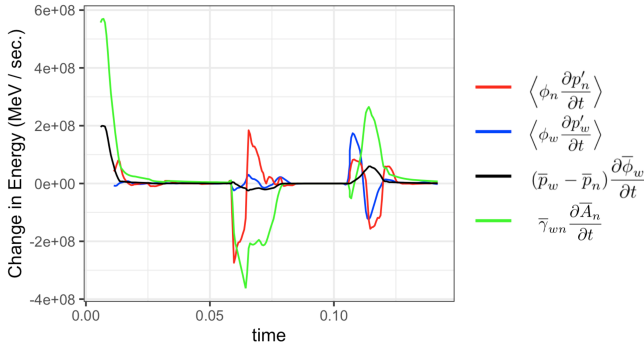


FIG. 5. Contribution of energy terms based on typical pore-scale events for drainage and imbibition in porous media.

The energy associated with pressure fluctuations that arise due to pore-scale events is shown in Fig. 5. At the pore level, the energy due to fluctuations is comparable to the rate of pressure volume work and the rate of change in surface energy. Defining the exchanges between these terms in a non-equilibrium setting is non-trivial. It is clear from these results that the fluctuation terms contribute a significant amount to the overall energy dynamics at the scale of an individual pore. We now extend this analysis to larger scale systems where large numbers of pore-scale events occur, allowing their frequency and distribution to be analyzed in detail.

Experimental Results

Experimental data was collected for a Berea sandstone. The sample porosity was 0.199 and the absolute permeability was $0.7 \mu\text{m}^2$. The sample diameter was 4 mm and the length 10 mm. Oil was injected into the sample at a rate of $0.35 \mu\text{L}/\text{minute}$. Pressure transducer measurements were collected for the oil at an interval of $\Delta t = 0.32$ sec. Several assumptions were necessary to support the analysis of the experimental data. since Pressure mea-

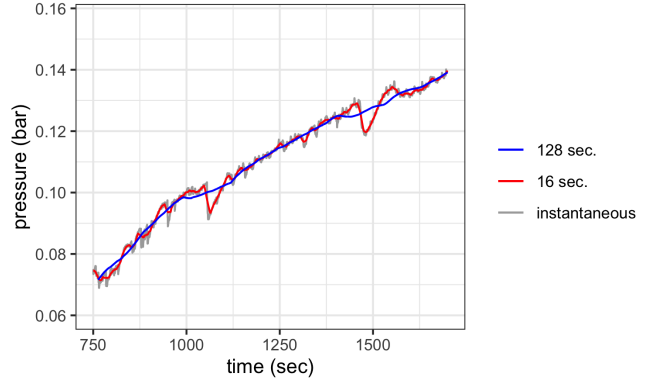


FIG. 6. Experimental pressure signal from primary drainage in a sandstone with time-averaged pressures obtained based on a time interval of 16 s. and 128 s. Time-averaging smooths the fluctuations in the pressure signal; the associated contributions to the energy are linked with the fluctuation terms.

surements were available for the oil phase only, the water was assumed to be in equilibrium with the external pressure (1 atm) at the outlet of the sample. Since the transducer measurements for the oil pressure are available only at the inlet boundary, this was assumed to adequately represent the spatially averaged pressure within the sample. While it is nearly certain that various intermittent pressure gradients and spatial fluctuations occurred within the sample, the response of the pressure waves (based on the speed of sound) is fast compared to the timescale for flow (based on the rate of change in saturation). Time derivatives were evaluated by fitting a spline function to the experimental time series data and evaluating the first derivative. Time averages were then computed based on a simple moving average (SMA). Average pressure values are shown in Fig. 6.

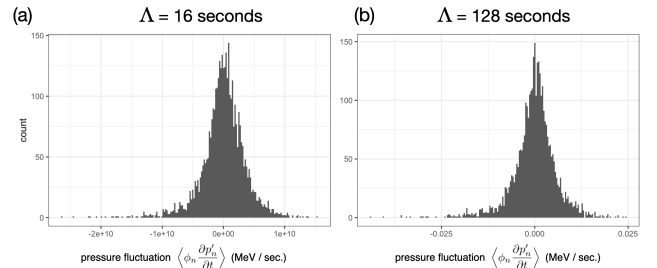


FIG. 7. Observed distribution for pressure fluctuation determined using experimental data with the temporal averaging interval (a) $\Lambda = 16$ sec. (b) $\Lambda = 128$ sec.

Fig. 7 shows the experimental pressure signal and time-averaged curves computed based two time intervals, $\Lambda = 16$ seconds and $\Lambda = 128$ seconds. Pressure fluctuations continue to be evident due to the larger events with $\Lambda = 16$ sec. These fluctuations are mostly removed for $\Lambda = 128$ sec, although the effect of larger events re-

mains visually evident. Time average effectively removes the noise due to the fast pressure fluctuations from the pressure signal. The contributions of the pressure fluctuation terms is accounted for based on the fluctuation terms identified in Eq. 43. The distribution for the pressure fluctuation is shown in Fig. 7. Since the pressure fluctuation is defined based on the difference between the instantaneous and average pressure values, the amplitude is sensitive to the averaging interval. Fig. 7 (a) shows the distribution for $\Lambda = 16$ seconds. The distribution for $\Lambda = 128$ seconds. is shown in Fig. 7 (b). According to the central limit theorem, the distribution should be well-approximated by the Gaussian distribution provided Λ is large enough to include a sufficiently large number of pore-scale events. Assumption also requires that the average pressure \bar{p}_i be stationary; if the average pressure pressure value is drifting in time, then skew may be introduced in the pressure fluctuation distribution. This is an effective condition for the REV of the system. As the system grows larger, the rate of change to the fluid volume fraction $\partial\bar{\phi}_w/\partial t$ will be slower, since it takes a longer time for flow to fill the larger system. However, the timescale for pore-scale events will be the same. The average pressure signal will tend to be more stationary for larger systems considered over longer time intervals. For a fixed system size, a larger Λ will smooth the pressure signal and reduce the amplitude of the pressure fluctuations, as shown in Fig. 8. However, a larger value of Λ will mean the distribution is less stationary, since the average pressure can drift more over a longer time interval. For example, it is clear from Fig. 6 that the average pressure difference is changing at the timescale for $\Lambda = 128$.

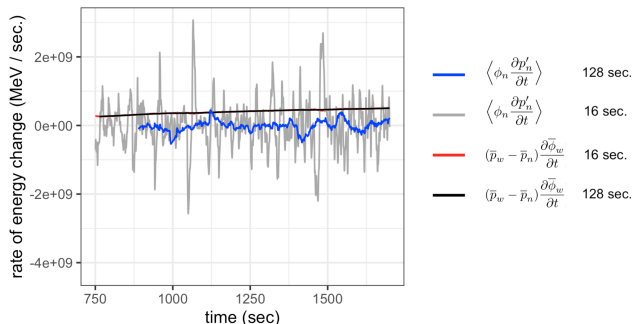


FIG. 8. The amplitude of pressure fluctuations is reduced based on the interval for time averaging. As the time interval for averaging is increased, fluctuations become less significant as compared to the rate of pressure volume work.

A reasonable criterion for the REV is that the magnitude for the pressure fluctuations (based on the variance for the pressure fluctuation distribution as depicted in Fig. 7) must be small as compared to the rate of pressure-volume work. If this condition is not met, then *rheons* will exert an asymmetric influence on the pressure signal

and Eq. 50 will not hold. In this situation, the average energy landscape is “rugged” in nature and the fluctuations must be considered explicitly. In a sufficiently large system, considered over a sufficiently large time interval, Eq. 50 should hold and an averaged non-equilibrium description may be possible. Fig. 8 shows the amplitude of pressure fluctuations on the energy scale, which includes the rate of pressure-volume work. The instantaneous values for the pressure fluctuation can be very large, due to the fact that pore-scale events are very fast. The overall energy contribution is significant, and cannot be ignored unless REV requirements are met. It is possible that Eq. 50 may counter-balance for some asymmetry in the pressure fluctuations, since this condition can still be met if pressure fluctuation energy is redistributed to the surface energy. This effectively means that some part of the average energy from *rheons* can be reversibly transferred to surface energy. In this situation the dissipative parts must still be accounted for from Eqs. 3 and 54.

Spectral analysis for capillary fluctuations is shown in Fig. 9. Time averaging intervals were varied from $\Lambda = 8$ seconds to $\Lambda = 512$ seconds, which reduce the amplitude of fluctuations due to cancellation. However, the underlying signature of the noise spectrum remains essentially unchanged based on the temporal averaging window. We find that the spectral power density is S_P predicted from the frequency F based on the equation

$$\log S_P \sim \alpha F^p . \quad (56)$$

The coefficients $\alpha = -15$ and $p = 1/2$ are consistent with results obtained for droplet coalescence [49]. Within the pink region, the capillary fluctuations produce noise that is consistent with pink noise $S_P \sim 1/F$, which is consistent with self-organized critical behaviour [69]. However, there is an upper bound on the frequency for capillary fluctuations due to length scale effects. The decay of the S_P at faster frequencies is linked with the relaxation timescale associated with porescale events [3, 23]. Due to the time required to fill an individual pore, the probability of fast events decreases rapidly for sufficiently fast frequencies, as in the red region. The yellow region corresponds to longer frequencies that may be inaccessible due to system size effects.

An assessment of the temporal REV is shown in Fig. 10. Assessment of the REV based on the pressure fluctuations must consider two essential components: (1) the mean for the pressure fluctuation distribution, since a non-zero mean implies there is a net contribution to the internal energy; (2) the variance associated with the amplitude of the pressure fluctuation, which is related to the number of pore-scale events within the time interval Λ . For the particular experimental data considered here, the energy associated with the mean pressure fluctuation is $\sim 5\%$ of the rate of pressure-volume work. This can likely only be further reduced by increasing the physical size of the sample. The standard deviation for the

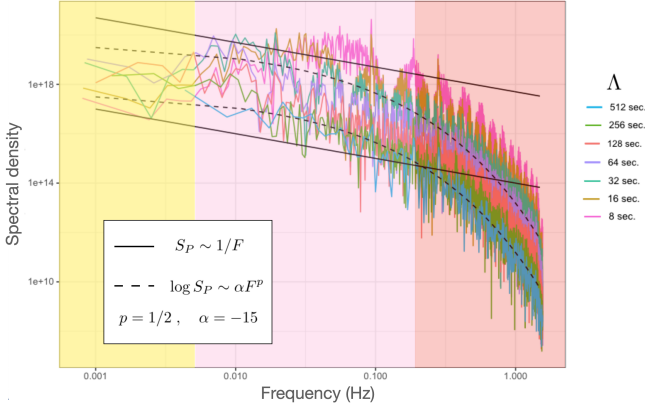


FIG. 9. Power spectral density for the pressure fluctuation based on experimental drainage data for a range of averaging intervals from $\Lambda = 8$ seconds to $\Lambda = 512$ seconds. The time averaging interval alters the amplitude of fluctuations but not the frequency signature.

pressure fluctuation decreases as Λ increases, decreasing to ~ 10 percent of the rate of pressure-volume work for $\Lambda = 512$ seconds. When considered over short time averaging intervals the fluctuations are several times the rate of pressure volume work. Based on the metrics defined in Fig. 10 the REV accuracy for the experimental system considered is likely to be in the range of $\pm 5\text{--}10\%$ for the capillary pressure. It is noted that the requirement given in Eq. 50 can still be satisfied if the net contribution from the pressure fluctuation balances against the change in surface energy and the contribution due to film swelling. However, this cannot be assessed for the data set considered here, since the data needed to evaluate the curvature and film contributions was not collected. Additional study of this relationship is important, since the rate of change in curvature cannot be independent from other terms in the flux-force form of the entropy inequality. Independence is a requirement to derive Eq. 54, which is why Eq. 50 must hold to derive phenomenological equations.

It is important to recognize that pore-scale events will always dissipate a significant amount of energy during two-fluid flow in porous media. Averaging does not change this. What averaging does accomplish is to treat fluctuations such that their energy dissipation is accounted for based on Eqs. 3 and 54, i.e. in situations where Eq. 50 is satisfied. The constitutive models for relative permeability and dynamic capillary pressure are not valid if these constraints are not met. However, when the system size is large and long time intervals are considered, the net contribution of the capillary fluctuation terms will trend towards zero. Their role on dissipation within the system will then be incorporated into the phenomenological coefficients k_{rn} , k_{rw} and τ_w .

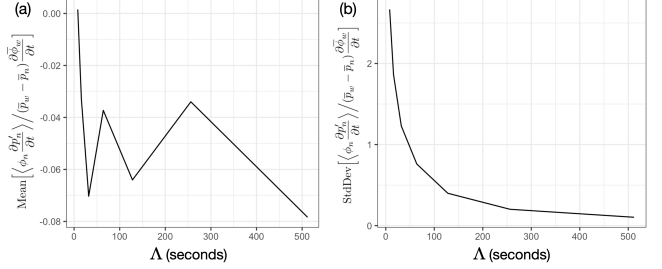


FIG. 10. Temporal REV assessment for experimental data by comparing the energy due to fluctuations with the rate of pressure volume work: (a) due to the change in the capillary pressure and volume fraction over the averaging interval Λ , fluctuations have non-zero mean value. Fluctuations will tend to have mean value closer to zero in spatially larger systems or when Λ is smaller; (b) standard deviation for fluctuations decreases toward zero as the time interval Λ increases, such that many pore-scale events are factored into the averages.

SUMMARY

We derive non-equilibrium thermodynamics for immiscible fluid flow in porous media using the method of time-and-space averaging. Averaging in both time and space reveals macroscopic thermodynamic fluctuation terms, which are athermal in nature and account for fluctuations due to multi-scale effects such as capillary pressure dynamics. An entropy production equation is derived that includes the relevant fluctuation terms, which is converted into flux-force form to support the derivation of phenomenological equations. The standard equations for effective permeability can be derived, which can be generalized to cross-coupling forms in situations where significant momentum exchanges occur between fluids. Key results of the theory are (1) a REV constraint on “slow” fluctuations observed during steady-state displacement, which is needed to derive the flux-force form of the entropy inequality; and (2) a dynamic capillary pressure expression that includes the effects of films and capillary fluctuations. Using simulation and experimental data we show that capillary fluctuations represent a significant part of the non-equilibrium energy dynamics for immiscible fluid flow. Based on experimental data, we assess the distribution for capillary fluctuations for time intervals ranging from $\Lambda = 8$ seconds to $\Lambda = 512$ seconds. We show that the power spectrum for fluctuations can be characterized by a simple scaling law. The net contribution for fluctuations during unsteady displacement varies from 5–10% of external pressure-volume work. Our results indicate that capillary fluctuations are an essential consideration to determine REV for immiscible fluid flow. Further work is needed to evaluate constitutive models for the dynamic capillary pressure in different types of porous media.

Acknowledgements

‘An award of computer time was provided by the Department of Energy Summit Early Science program. This research also used resources of the Oak Ridge Leadership Computing Facility, which is a DOE Office of Science User Facility supported under Contract DE-AC05-00OR22725.

-
- [1] R.T. Armstrong and S. Berg, *Phys. Rev. E*, **88**, 043010, (2013).
- [2] S. Berg, H. Ott, S.A. Klapp, A. Schwing, R. Neiteler, N. Brussee, A. Makurat, L. Leu, F. Enzmann, J. Schwarz, M. Kersten, S. Irvine, M. Stampanoni, *PNAS*, **110**, 3755, (2013).
- [3] R.T. Armstrong, H. Ott, A. Georgiadis, M. Rücker, A. Schwing A, and S. Berg, *Water Resour Res* **50** 9162 (2014).
- [4] L. Cueto-Felgueroso, R. Juanes. *Geophysical Research Letters* **43**, 1615 (2015)
- [5] N.R. Morrow, *Ind. Eng. Chem* **63**, 32 (1970).
- [6] B. K. Primkulov, A.A. Pahlavan, X. Fu, B. Zhao, C.W. MacMinn and R. Juanes, *Journal of Fluid Mechanics* **875**, R4 (2019).
- [7] M. Winkler, M.a. Gjennestad, D. Bedeaux, S. Kjelstrup, R. Cabriolu, R. and A. Hansen, *Frontiers in Physics*, **8**, 60 (2020).
- [8] F. S. Gnesotto, F. Mura, J. Gladrow, and C.P. Broedersz, *Reports on Progress in Physics*, **81** 066601 (2018).
- [9] L. Onsager, *Phys. Rev.* **37**, 405 (1931).
- [10] S.R. de Groot and P. Mazur, (Dover, Amsterdam, 1984).
- [11] S.M. Hassanizadeh and W.G. Gray, *Adv. Water Res.*, **16**, 53 (1993).
- [12] S. Kjelstrup, D. Bedeaux, A. Hansen, B. Hafskjold and O. Galteland, arXiv preprint arXiv:1805.03943 (2019)
- [13] W.G. Gray and C.T. Miller, “Introduction to the Thermodynamically Constrained Averaging Theory for Porous Medium Systems,” (Springer, Zürich, 2014).
- [14] J. Bear and J.J., Nitao, *Transp Porous Med* **18**, 151 (1995).
- [15] Marle, C., “Multiphase Flow in Porous Media”, Editions Technip (1981).
- [16] J. Xu, S. Kjelstrup, D. Bedeaux, A. Røsjorde, L. Rekvig *Journal of Colloid and Interface Science* **299**, 452 (2006).
- [17] , H.A. Bethe and E. Teller, (No. NP-4898; BRL-X-117). Engineering Research Institute, University of Michigan (1953).
- [18] Y. Li, C. Garing and S.M. Benson, *Journal of Fluid Mechanics* **889** A14 (2020).
- [19] I. Battiato, D.M. Tartakovsky, *Journal of Contaminant Hydrology*, **120–121**, 18 (2011).
- [20] I. Battiato, D.M. Tartakovsky, A.M. Tartakovsky, T. Scheibe, *Advances in Water Resources*, **32**, 1664 (2009).
- [21] J.H. Cushman and T.R. Ginn, *Transp Porous Med* **13**, 123 (1993).
- [22] J. H. Cushman and D. O’Malley, *Journal of Hydrology*, **531**, 161 (2015).
- [23] S. Schlüter, Berg, S., Li, T., Vogel, H.-J., and Wildenschild, D. *Water Resour. Res.*, **53**, 4709 (2017).
- [24] McClure, J.E., Ramstad, T., Li, Z. Armstrong, R.T., Berg, S. *Transp Porous Med* **133**, 229 (2020).
- [25] M. Orme, *Progress in Energy and Combustion Sci.* **23**, 65 (1997).
- [26] J. Toro-Mendoza, O. Paredes-Altuve, M.A. Velasquez and D.N. Petsev *Phys. Rev. Fluids* **4**, 093604 (2019).
- [27] M. Wu *Physics of Fluids* **16**, L51 (2004).
- [28] W. D. Ristenpart, P. M. McCalla, R. V. Roy, and H. A. Stone *Phys. Rev. Lett.* **97**, 064501 (2006).
- [29] Dirk G. A. L. Aarts, Henk N. W. Lekkerkerker, Hua Guo, G.H. Wegdam, D. Bonn *Phys. Rev. Lett.* **95**, 164503 (2005).
- [30] J.D. Paulsen, R. Carmigniani, Anerudh Kannan, Justin C. Burton, and Sidney R. Nagel, *Nat. Commun.* **5**, 3182 (2014).
- [31] J.D. Paulsen, J.C. Burton, S.R. Nagel, S. Appathurai, M.T. Harris, O.A. Basaran, *PNAS* **109**, 6859 (2012).
- [32] J.D. Paulsen, J.C. Burton, S.R. Nagel, *Phys. Rev. Lett.* **106**, 114501 (2011).
- [33] S. C. Case and S. R. Nagel, *Phys. Rev. Lett.* **100**, 084503 (2008).
- [34] C.Y. Pak, W. Li, Y-L. Tse, *Journal of Physical Chemistry*, **122**, 22975 (2018).
- [35] X. Li, H. Ren, W. Wu, H. Li, L. Wang, Y. He, J. Wang and Y. Zhou, *Scientific Reports*, **5**, 15190 (2015).
- [36] H. Vahabi, W. Wang, J.M. Mabry and A.K. Kota, *Science Advances*, **4**, 3488 (2018).
- [37] A.A. Pahlavan, H.A. Stone, G.H. McKinley and R. Juanes *Proceedings of the National Academy of Sciences* **116** (28), 13780 (2019).
- [38] S. Perumananth, M.K. Borg, M.V. Chubynsky, J.E. Sprittles, J.M. Reese, *Physical Review Letters*, **122**, 104501 (2019).
- [39] J.G. Roof *SPEJ* **10**, 85 (1970)
- [40] W. B. Haines, *J. Agric. Sci.*, **20**, 97, (1930).
- [41] A.W. Adamson and A.P. Gast, “Physical Chemistry of Surfaces,” (Wiley, Hoboken, 1997).
- [42] S. Seth and N.R Morrow, *SPE Reservoir Evaluation & Engineering* 102490 (2007).
- [43] W.G.Gray,A.L. Dye, J.E. McClure, L. J. Pyrak-Nolte and C.T.Miller, *Water Resour. Res.*, **51**, 5365 (2015).
- [44] S. Kjelstrup and D. Bedeaux, “Non-Equilibrium Thermodynamics of Heterogeneous Systems,” (World Scientific, Hackensack, 2008)
- [45] O. Galteland, D. Bedeaux, S. Kjelstrup and B. Hafskjold, *Frontiers in Physics* **7**, 60, (2019).
- [46] K. K. Mohanty, H. T. Davis and L.E. Scriven, *Society of Petroleum Engineers* **2**, 113 (1987).
- [47] D.A. DiCarlo, J.I.G Cidoncha and C. Hickey, *Geophysical Research Letters*, **30**, 1901 (2003).
- [48] S.A. Aryana and A.R. Kovscek, *Transp. Porous Med.* **97**, 373 (2013).
- [49] J.E. McClure, S. Berg and R.T. Armstrong, arXiv **TBD**, TBD (2020).
- [50] S. Whitaker, *Transp Porous Med* **1**, 105 (1986).
- [51] P. Purswani, M.S. Tawfik, Z.T. Karpyn, R.T. Johns *Computational Geosciences*, **24**, 807 (2019).
- [52] B. Amaziane, J.P. Milisic, M. Panfilov, and L. Pankratov, *Phys. Rev. E*, **85**, 016304 (2012).
- [53] R. Lenormand, E. Touboul, C. Zarcone *J. Fluid Mech.* **189** 165-187, 1988
- [54] M. Rücker, S. Berg, R. T. Armstrong, A. Georgiadis, H. Ott, A. Schwing, R. Neiteler, N. Brussee, A. Makurat, L. Leu, M. Wolf, F. Khan, F. Enzmann, M. Kersten *Geo-*

- physical Research Letters 42, 3888-3894, (2015).
- [55] J.E. McClure, R.T. Armstrong, M.A. Berrill, S. Schlüter, S. Berg, W.G. Gray, C.T. Miller, *Phys. Rev. Fluids* **3** 084306 (2018).
- [56] S. Schlüter, S. Berg, S. M. Rücker, R.T. Armstrong, H.-J. Vogel, R. Hilfer, D. Wildenschild, *Water Resour. Res.*, **52**, 2194-2205 (2016)
- [57] C.S. Land *SPEJ*, **8**, 149, (1968).
- [58] R.J. Lenhard, J.C. Parker *Water Resour. Res.*, **23**, 2197, (1987).
- [59] R. Hilfer, *Phys. Rev. E*, **73**, 016307 (2006).
- [60] Z. Liu, A. Herring, C. Arns, S. Berg, and R.T. Armstrong, *Transp. Porous Media*, 1, (2017).
- [61] R.T. Armstrong, J.E. McClure, M.A. Berrill, M. Rücker, S. Schlüter, S. Berg, *Phys. Rev. E*, **94**, 043113 (2016).
- [62] A.L. Herring, E.J. Harper, L. Andersson, A. Sheppard, B.K. Bay, D. Wildenschild, *Adv. Water Res.*, **62**, 47, (2013).
- [63] J.E. McClure, M.A. Berrill, W.G. Gray, and C.T. Miller, *Phys. Rev. E*, **94**, 033102 (2016).
- [64] W.G. Gray, A. Leijnse, "Mathematical tools for changing spatial scales in the analysis of physical systems," (CRC Press, Boca Raton, 1993).
- [65] J. E. McClure, Z. Li, M.A. Berrill, and T. Ramstad. *Computational Geosciences*, (accepted) 2020.
- [66] E. Veveakis, K. Regenauer-Lieb. *Current Opinion in Chemical Engineering* **7**, 40 (2015)
- [67] E.G. Flekkøy, S.R. Pride *Physical Review E* **60**, 4130 (1999)
- [68] F. O. Alpak, I. Zacharoudiou, S. Berg, J. Dietderich, N. Saxena *Computational Geosciences***23** 849 (2019).
- [69] P. Bak, C. Tang and K. Wiesenfeld, *Phys Rev Let.* **59** 381 (1987).